INORGANIC CHEMISTRY FRONTIERS

RESEARCH ARTICLE

View Article Online
View Journal | View Issue

Cite this: *Inorg. Chem. Front.*, 2023, **10**, 2039

A hybrid halide lead-free pseudo-perovskite with large birefringence†

Weiqi Huang,[a,c] Xiaolong Wu,[a,c] Belal Ahmed,[e] Yanqiang Li,[c] Yang Zhou,[c] Han Wang,[c] Yipeng Song,[c] Xiaojun Kuang,[b] Junhua Luo[c,d] and Sangen Zhao *[c,d]

Received 25th December 2022,
Accepted 8th February 2023

DOI: 10.1039/d2qi02738k

rsc.li/frontiers-inorganic

Birefringent crystals have important applications in optoelectronics due to their ability to modulate and polarize light. Hybrid halide perovskites were not considered as promising candidates for birefringent crystals until quite recently, when we reported a hybrid lead bromine perovskite with large birefringence. Herein, we report a novel lead-free hybrid pseudo-perovskite layered structure of $MLASnCl_4$ (MLA = melamine). Remarkably, $MLASnCl_4$ reveals a large birefringence of 0.294@550 nm, which is comparable to that of the previously reported hybrid lead bromine perovskite $MLAPbBr_4$. Furthermore, the surface morphologies of the reported crystals exhibit excellent air stability investigated by their exposure to air at room temperature for various time ranges. The observed birefringence is generated from the delocalized π-conjugations of melamine cations and stereochemically active lone pair electrons on the Sn^{2+} cations of highly distorted $SnCl_4$ tetrahedra, as suggested by theoretical calculations. This current research effort may open new windows for the design of hybrid perovskite materials for polarization-dependent optical applications.

Introduction

Birefringence is an important functional property of optical materials because of their unabated features of modifying the polarization of light.[1–5] Thus far, birefringent materials *e.g.*, α-BaB_2O_4 (0.122@546 nm),[6] $LiNbO_3$ (0.074@546 nm),[7] YVO_4 (0.204@532 nm),[8] $CaCO_3$ (0.172@532 nm),[9] and TiO_2 (0.256@546 nm)[10] have been broadly applied in commercially available optical devices. The established birefringent materials are inadequate to fulfill the demand for optical materials in the applied field due to their relatively high cost, high energy consumption for crystal growth, and lack of crystal quality.

In particular, several π-conjugated groups were effectively introduced for the design of birefringent materials *e.g.*, $(C_3N_3O_3)^{3-}$ (cyanurate), $(BO_3)^{3-}$, $(B_2O_5)^{4-}$, $(B_3O_6)^{3-}$, $(NO_3)^-$, and $(CO_3)^{2-}$.[11–16] Among them, the well-known commercial material α-BaB_2O_4 exhibits a relatively large birefringence, which originated from the electronic contribution of the 6-membered anionic $(B_3O_6)^{3-}$ group. Recently, a series of compounds containing $(C_3N_3O_3)^{3-}$ groups have been successfully explored.[17] In addition, compound $2(C_3H_7N_6)^+2Cl^-{\cdot}H_2O$ with large birefringence was investigated through the incorporation of functional melamine cations.[18] The birefringence of this compound could increase due to the introduction of a planar 6-membered π-conjugated melamine group which acts as a birefringent chromophore. The structural configuration of the $(C_3N_6)^{6-}$ (melamine) unit is similar to that of the $(B_3O_6)^{3-}$ and $(C_3N_3O_3)^{3-}$ groups.

The introduction of two or more birefringent chromophores could be a promising strategy to explore novel optical functional perovskite materials.[19–21] In particular, the combination of planar π-conjugation systems and transition metal cations with stereochemically active lone pair electrons in a parallel arrangement could be an excellent strategy to enhance the birefringence of materials.[22–24] A new phosphate compound, Sn_2PO_4I, with a large birefringence was reported. Theoretical calculations suggest that the stereochemically active lone pair electrons on the Sn^{2+} cation might enhance the birefringence of Sn_2PO_4I.[25] The reported inorganic perovskite material

[a]College of Chemical Engineering, Fuzhou University, Fuzhou 350116, China
[b]College of Materials Science and Engineering, Guilin University of Technology, Guilin 541004, China
[c]State Key Laboratory of Structural Chemistry, Fujian Institute of Research on the Structure of Matter, Chinese Academy of Sciences, Fuzhou 350002, China
[d]Fujian Science & Technology Innovation Laboratory for Optoelectronic Information of China, Fuzhou 350108, China
[e]Department of Chemistry, Shahjalal University of Science and Technology, Sylhet-3114, Bangladesh

†Electronic supplementary information (ESI) available: Crystal photograph, powder XRD patterns, TG-DTA curves, UV-Vis-NIR diffuse reflectance spectroscopy, *etc*. CCDC 2224808. For ESI and crystallographic data in CIF or other electronic format see DOI: https://doi.org/10.1039/d2qi02738k

Cs_4PbBr_6 containing $CsPbBr_3$ nanocrystals suggested that employing transition metals with lone pair electrons would also be a potential strategy for designing birefringent crystals.[1] Recently, the hybrid perovskite structure $MLAPbBr_4$ with an experimental birefringence value of 0.322@550 nm was reported by our research group. The observed birefringence of this compound was relatively large despite the absence of stereochemically active lone pair electrons on Pb^{2+} cations.[26] Hence, the development of novel hybrid perovskite compounds with large birefringence is still attractive in various applied fields.

To avoid the toxicity of the Pb element and the stereochemical inertness of the Pb^{2+} cation in the symmetric coordination environment, we focused on the development of lead-free novel hybrid perovskite materials with birefringence properties. A new 2D hybrid pseudo-perovskite layered structure of $MLASnCl_4$ (MLA = melamine) was successfully synthesized by incorporating the planar π-conjugated melamine cations and the stereochemically active Sn^{2+} cations into halide systems.

Experimental section

Synthesis

$C_6H_6N_6$ (melamine) (Alfa Aesar, 99%), $SnCl_2$ (Aladdin, 99%), HCl (aq. 37 wt%), and hypophosphorous acid (H_3PO_2) (AR, aq. 50 wt%) were used as reagents without further purification. Melamine and $SnCl_2$ (1 : 1 molar ratio) were mixed in concentrated HCl solution with hypophosphorous acid. The mixture was heated and a colorless clear solution was obtained since the starting reagents are easily dissolved in an aqueous HCl solution. The hot solution was put in the fume hood and naturally cooled down to room temperature. Then, colorless transparent flake-like crystals of $MLASnCl_4$ (MLA = melamine) were precipitated from the solution. Hypophosphorous acid acts as a reducing agent in the synthesis process, which inhibits the conversion of Sn(II) to Sn(IV).

Results and discussion

The crystal structure of $MLASnCl_4$ was determined by single-crystal X-ray diffraction (XRD) analysis, which shows that it crystallizes in the non-centrosymmetric orthorhombic crystal space group $Pna2_1$ with cell parameters of a = 21.8661(7) Å, b = 6.0217(2) Å, c = 17.5955(5) Å, $\alpha = \beta = \gamma = 90°$, Z = 8, and V = 2316.82(13) $Å^3$ (detailed crystallographic information is provided in Tables S1–S5†). The structural unit consists of melamine cations and $SnCl_4$ tetrahedra (Fig. 1a). The melamine cations in the crystal structure of $MLASnCl_4$ are not arranged in a completely parallel arrangement. Adjacent melamine planes have a dihedral angle of approximately 61° (Fig. S1†). The Sn atom is coordinated by four chlorine atoms, forming a $[SnCl_4]^{2-}$ seesaw with Sn–Cl bond lengths of 2.517(2)–2.980(3) Å. The $[SnCl_4]^{2-}$ seesaw is in a highly distorted environment

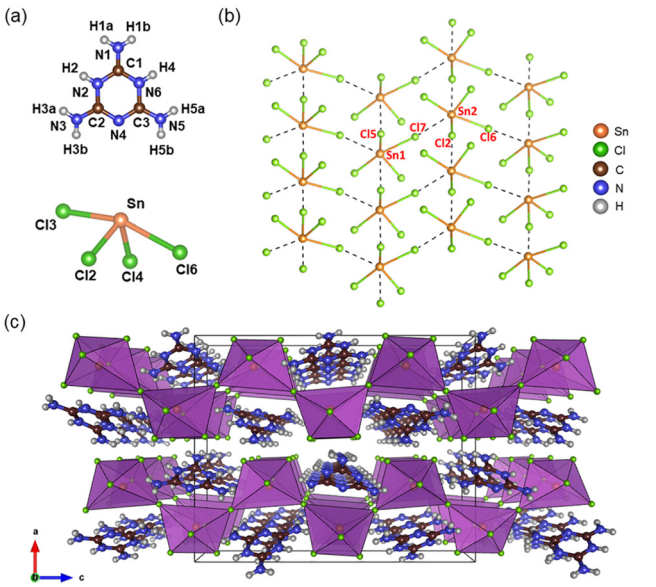

Fig. 1 Ball-and-stick and the polyhedral model representing (a) protonated MLA^{2+} cations and $[SnCl_4]^{2-}$ tetrahedra. (b) The 2D extended layer structure of $MLASnCl_4$ along the b-axis. (c) Pseudo-perovskite layered structure of $MLASnCl_4$ presented along the b-axis. The $SnCl_6$ octahedra are represented as purple-colored polyhedra.

owing to the lone pair on the Sn^{2+} cation, and the distorted $[SnCl_4]^{2-}$ tetrahedra are also not aligned parallel to each other. Adjacent $[SnCl_4]^{2-}$ seesaws are almost vertical to each other. The Sn^{2+} cations in $[SnCl_4]^{2-}$ interact with Cl2, Cl5, Cl6, and Cl7 in the adjacent $[SnCl_4]^{2-}$ tetrahedra with four Sn1–Cl5, Sn1–Cl6, Sn2–Cl2, and Sn2–Cl7 bonds with distances of 3.551 (3) Å, 3.402(3) Å, 3.523(3) Å, and 3.278(3) Å, respectively, which results in an infinitely extendable 2D pseudo-perovskite layer (Fig. 1b). Thus, the structure of $MLASnCl_4$ can be described as a pseudo-peroxide, which consists of corrugated $[SnCl_4]_\infty$ layers and interlayer melamine cations with N–H–Cl hydrogen bonds connecting the melamine cations and inorganic layers (Fig. 1c). The arrangement of both planar melamine cations and distorted $[SnCl_4]^{2-}$ tetrahedra in the structure is not conducive to the production of large birefringence.

The photograph of the synthesized colorless transparent single crystals is presented (Fig. S2†). The measured powder X-ray diffraction (PXRD) data are consistent with the calculated data, which ensures that the reported compound is pure (Fig. S3†). The mapping of SEM analysis shows that elements Sn, Cl, N, and, C are uniformly allotted in the compound crystals (Fig. 2a). Besides, the energy-dispersive X-ray (EDX) data confirm the observed elemental ratios of 1 : 4.25 for Sn and Cl with the stoichiometric ratios in the title compound (Fig. S4†). The PXRD patterns of the samples after being exposed to air for two weeks were measured at room temperature, which show a good match with the original PXRD pattern of the compound (Fig. 2b). Moreover, the surface morphologies of the single crystals of the compound remain unchanged after exposing the samples to air at room temperature for various

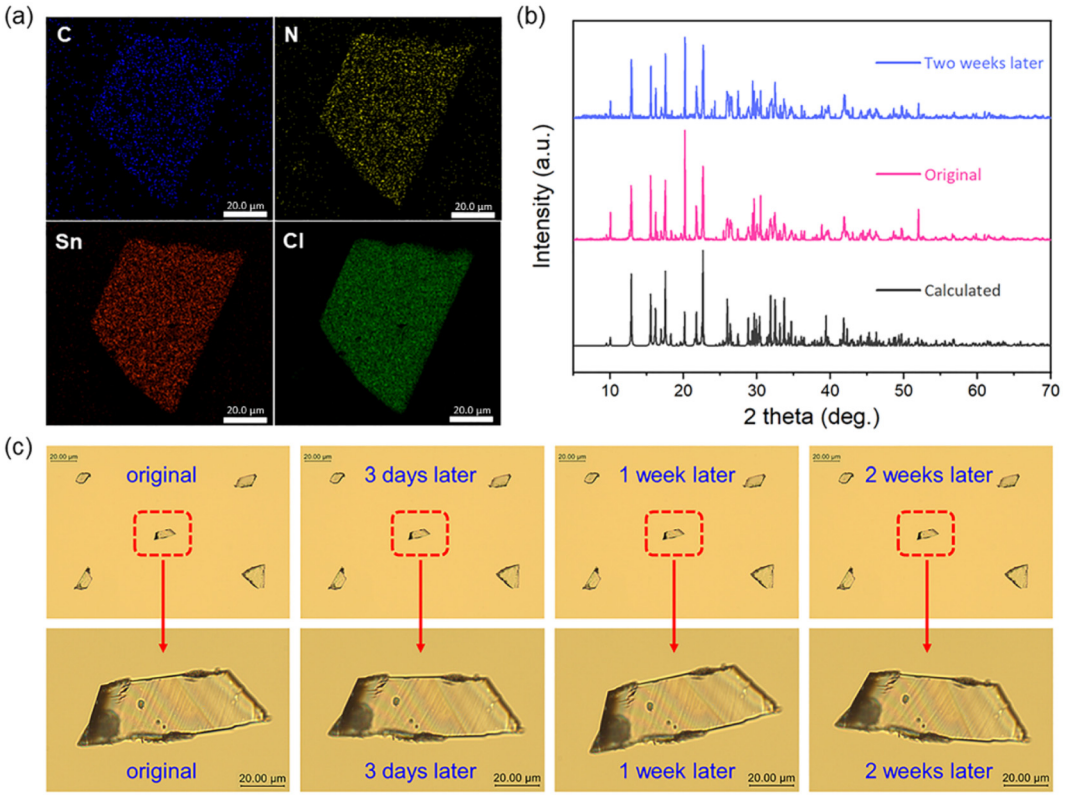

Fig. 2 (a) The mapping of elemental SEM analysis in a single crystal. (b) The measured PXRD pattern for samples exposed to air and the calculated PXRD pattern for $MLASnCl_4$. (c) The surface morphologies of the single crystals of the compound exposed to air at room temperature for various time ranges. Single crystals are highlighted with dashed red boxes for magnified observation.

time ranges, such as three days, one week, and two weeks, respectively (Fig. 2c). Based on this experimental observation, it is noted that the crystals of the reported $MLASnCl_4$ perovskite exhibit excellent air stability. Recently, 2D perovskite materials consisting of organic cations and tin metal have been explored, in which π-electron rich organic ligands could become a significant factor for the stability of materials.[27–29] The synthesized compound may prevent the interaction with oxygen and water molecules owing to the presence of π-conjugated bulky hydrophobic melamine cations. In addition, the intermolecular interactions between melamine cations with π-conjugation systems should be stabilized by the crystal structure through the improvement of intrinsic stability.

The compound $MLASnCl_4$ which maintains a stable structure up to 450 K is investigated by thermogravimetric (TG) and differential thermal analysis (DTA) diagrams (Fig. S5†). Above this temperature, this compound exhibits weight losses due to the release of lattice water molecules, which is revealed through the corresponding endothermic peak.

The ultraviolet–visible–near-infrared (UV–Vis–NIR) diffuse reflectance spectrum of $MLASnCl_4$ was recorded in the wavelength region of 200–800 nm. The result indicates that the observed bandgap for this compound is *ca.* 3.71 eV, and that of the corresponding UV absorption edge is 334 nm (Fig. S6†).

The IR spectrum of $MLASnCl_4$ is depicted in Fig. S7† to help verify the main functional groups and chemical bonds. The sharp absorption peaks in the range of 760–1700 cm^{-1} represent the asymmetric stretching vibrations and the out-of-plane bending vibration of the C–N side chain in the melamine ring. The strong absorption bands in the range of 3000–3300 cm^{-1} correspond to the asymmetric and symmetric stretching vibrations of $[NH_2]$. However, the absorption bands of the $[SnCl_4]^{2-}$ vibration are not observed in the experimental IR spectrum as they always appear below 500 cm^{-1} in IR.

A polarizing microscope was employed to estimate the birefringence of $MLASnCl_4$. Fourth-order pink color is observed for the original interference of $MLASnCl_4$ crystals under orthogonally polarized light, which can be achieved from full extinction (Fig. 3a and b). The thickness of the crystal is found to be *ca.* 9.6 μm (Fig. S8†) and the observed optical path difference is 2.823 μm at 550 nm. The birefringence was measured on the (010) plane of the crystal based on the SCXRD analysis of the sample (Fig. S9†). The refractive index difference was determined on the crystalline (010) plane using the formula listed in the ESI† and the observed refractive index difference value is *ca.* 0.294. The experimental birefringence value *ca.* 0.294@550 nm of $MLASnCl_4$ closely matches the reported values of materials, such as $MLAPbBr_4$ (0.322@550 nm),[26] $(C_9H_{14}N)SbCl_4$ (0.095@546 nm),[30] and $CsPbI_3$ (0.275@1064 nm).[31] In addition, the observed birefringence value

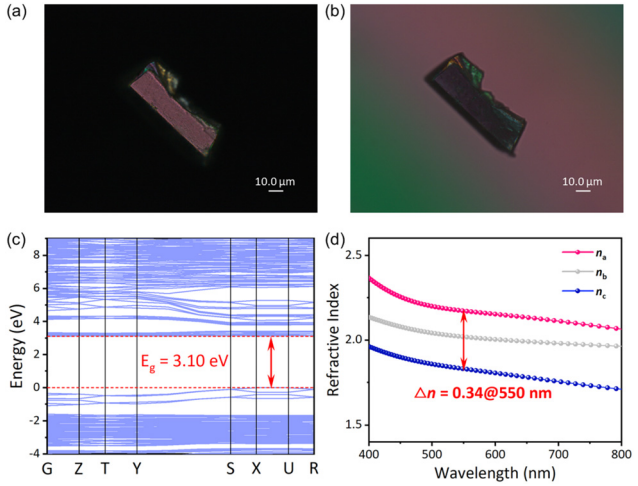

Fig. 3 (a) Under orthogonally polarized light, fourth-order pink color is observed for $MLASnCl_4$. (b) The complete extinction of $MLASnCl_4$ crystals. (c) Electronic band structure for $MLASnCl_4$ obtained from theoretical calculations. (d) Wavelength-dependent refractive indices with the birefringence value of $MLASnCl_4$.

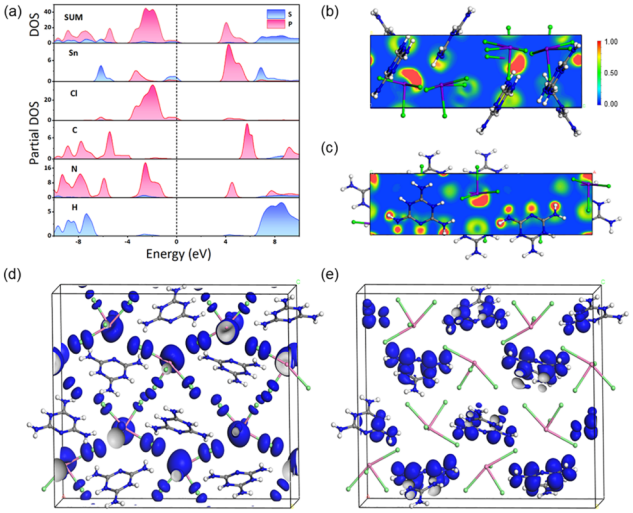

Fig. 4 (a) DOS and partial DOS of $MLASnCl_4$. 2D ELF diagram of $MLASnCl_4$ represents the slice cutting through Sn atoms in (b) the (100) plane and (c) the (001) plane. The iso-value is changed from blue to red which represents an increase from 0 to 1. (d) The HOMO for $MLASnCl_4$. (e) The LUMO for $MLASnCl_4$ (purple, Sn; green, Cl; grey, C; blue, N; and white ball, H).

of $MLASnCl_4$ is larger than the values of earlier reported birefringent materials, *e.g.*, α-BaB_2O_4 (0.122@532 nm),[6] YVO_4 (0.204@532 nm),[8] $CaCO_3$ (0.172@532 nm),[9] and TiO_2 (0.256@546 nm).[10]

The electronic band structure recommends that $MLASnCl_4$ exhibiting a direct band gap with a value of 3.10 eV is related to the experimental result (Fig. 3c). The theoretical birefringence value was determined through first-principles calculations based on density functional theory using the plane-wave pseudo-potential method including the CASTEP package.[32,33] The calculated birefringence value, Δn = 0.34@550 nm, for the wavelength-dependent refractive indices reflects a significant anisotropic environment in the compound. The calculated birefringence value of the compound agrees well with the value obtained from the experimental analysis (Fig. 3d).

To explain the origin of the observed birefringence for $MLASnCl_4$, additional theoretical calculations were performed. The diagrams of the density of states (DOS) and partial density of states (PDOS) for $MLASnCl_4$ show that the 3p, 2p, and 5p orbitals of Cl, N, and Sn atoms, respectively, dominate in the upper side of the valence band, whereas the 2p, 2p, and 5p orbitals of C, N, and Sn atoms, respectively, dominate in the lower side of the conduction band (Fig. 4a). The strong covalent bonding interactions of the C atom with the N atom are generated from the π-electron-rich melamine cations, as suggested by the DOS and PDOS diagrams. In addition, the observed Sn–Cl bonding interactions for $SnCl_4$ tetrahedra result from the strong overlaps between Sn 5p and Cl 3p orbitals near the Fermi level.

The electron localization function (ELF) diagram is used for the direct visualization of the electronic contributions from melamine cations and $SnCl_4$ tetrahedra in $MLASnCl_4$ (Fig. 4b and c). The resultant covalent networks between the C and N atoms in the melamine cations are found in both (100) and (001) planes. The anisotropic electron clouds around the Sn^{2+} cations are obviously observed, which represent that the lone pair electrons on the Sn^{2+} cations are stereochemically active. The highly distorted $SnCl_4$ tetrahedra in the compound are found to be attributable to the available lone pair electrons on the Sn^{2+} cations. This would explain why the lone pair of electrons of Pb^{2+} in the relatively symmetrically coordinated $MLAPbBr_4$ compound is stereochemically inert, whereas the title compound successfully introduced transition metal cations with stereochemically active lone pair electrons. Such resultant stereochemically active electron clouds may largely contribute to the birefringence of the reported compound. Moreover, analysis of the highest occupied molecular orbitals (HOMOs) and the lowest unoccupied molecular orbitals (LUMOs) of $MLASnCl_4$ was performed (Fig. 4d and e). The anisotropic electronic environments for highly distorted $SnCl_4$ tetrahedra and the highly π-conjugated delocalization for melamine cations are investigated by the HOMO and LUMO diagrams, respectively. Hence, both the distorted $SnCl_4$ tetrahedra with stereochemically active lone pair electrons on Sn^{2+} cations and melamine cations with delocalized π-conjugation could strongly contribute to the generation of large birefringence for $MLASnCl_4$.

The structure–property relationship suggests that the birefringence properties of materials are closely related to the anisotropic environments of structures, which potentially depends on the geometric arrangement of the birefringent chromophores.[34–37] The planar π-conjugated melamine groups in the structure of $MLASnCl_4$ are arranged with a large dihedral angle, which is attributable to the origination of a large

birefringence. In contrast, the π-conjugated anionic groups B_3O_6 and CO_3 have a parallel orientation in the structure of α-BaB_2O_4 and $CaCO_3$, respectively. It is noted that although the stereochemically active lone pair of electrons on Sn^{2+} cations contributes to the development of birefringence, the highly distorted $SnCl_4$ tetrahedra exhibit an anti-parallel orientation in the structure. This current research work may play an important role in designing new promising birefringent hybrid halide perovskites with toxic-free materials. The obtained highly stable, lead-free, and environmentally friendly birefringent crystals can be a potential candidate for material applications. Hence, a lot of research efforts might be still focused on the design and development of hybrid halide perovskite materials with a large birefringence.

Conclusions

In summary, a hybrid pseudo-perovskite layered compound $MLASnCl_4$ composed of corrugated infinite $[SnCl_4]^{2-}$ anions and melamine cations was synthesized through a facile aqueous solution method. The reported compound is highly air-stable and environmentally non-toxic compared to lead-based perovskites. The synthesized compound $MLASnCl_4$ shows a birefringence value of 0.294 at 550 nm, which originated from the distorted $SnCl_4$ tetrahedra with stereochemically active lone pair electrons on Sn^{2+} cations and the melamine ligand with delocalized π-conjugation. It is noticed that both melamine cations and $SnCl_4$ tetrahedra could not reveal the optimal structural anisotropy, so, additional research efforts might be still needed to increase the birefringence properties of hybrid halide perovskite materials.

Author contributions

W. Huang performed the main experimental work and paper writing. X. Wu, B. Ahmed, Y. Li, Y. Zhou, H. Wang, and Y. Song collected several experimental data. X. Kuang provided assistance with theoretical analysis. J. Luo and S. Zhao designed and supervised the overall experiments. All authors discussed and co-wrote the manuscript.

Conflicts of interest

The authors declare no competing interests.

Acknowledgements

This work acknowledges the financial support from the National Natural Science Foundation of China (22122507, 22193042, 21833010, 61975207, and 21921001), the Natural Science Foundation of Fujian Province (2022J02012), the Youth Innovation Promotion Association of the Chinese Academy of Sciences (Y202069), and the Key Research Program of Frontier Sciences of the Chinese Academy of Sciences (ZDBS-LY-SLH024), the Fujian Institute of Innovation (FJCXY18010201) in the Chinese Academy of Sciences, and the Key Laboratory of New Processing Technology for Nonferrous Metal & Materials, Ministry of Education/Guangxi Key Laboratory of Optical and Electronic Materials and Devices (20KF-11).

References

1 X. Chen, W. G. Lu, J. Tang, Y. Zhang, Y. Wang, G. D. Scholes and H. Zhong, Solution-processed inorganic perovskite crystals as achromatic quarter-wave plates, *Nat. Photonics*, 2021, **15**, 813–816.
2 S. Niu, J. Graham, H. Zhao, Y. Zhou, O. Thomas, H. Huaixun, S. Jad, M. Krishnamurthy, U. Brittany and J. Wu, Giant optical anisotropy in a quasi-one-dimensional crystal, *Nat. Photonics*, 2018, **12**, 392–396.
3 Z. Y. Xie, L. G. Sun, G. Z. Han and Z. Z. Gu, Optical Switching of a Birefringent Photonic Crystal, *Adv. Mater.*, 2008, **20**, 3601–3604.
4 Y. Zhou, Y. Li, Q. Ding, Y. Liu and J. Luo, Noncentrosymmetric $K_2Mn_3(SO_4)_3F_2{\cdot}4H_2O$ and $Rb_2Mn_3(SO_4)_3F_2{\cdot}2H_2O$ with pseudo-KTP structures, *Chin. Chem. Lett.*, 2020, **32**, 263–265.
5 Y. Zhou, X. Zhang, M. Hong, J. Luo and S. Zhao, Achieving effective balance between bandgap and birefringence by confining π-conjugation in an optically anisotropic crystal, *Sci. Bull.*, 2022, **67**, 2276–2279.
6 G. Zhou, J. Xu, X. Chen, H. Zhong and F. Gan, Growth and spectrum of a novel birefringent α-BaB_2O_4 crystal, *J. Cryst. Growth*, 1998, **191**, 517–519.
7 D. E. Zelmon, D. L. Small and D. Jundt, Infrared corrected Sellmeier coefficients for congruently grown lithium niobate and 5 mol% magnesium oxide –doped lithium niobate, *J. Opt. Soc. Am. B*, 1997, **14**, 3319–3322.
8 H. Luo, T. Tkaczyk, E. Dereniak and K. Oka, High birefringence of the yttrium vanadate crystal in the middle wavelength infrared, *Opt. Lett.*, 2006, **31**, 616–618.
9 G. Ghosh, Dispersion-equation coefficients for the refractive index and birefringence of calcite and quartz crystals, *Opt. Commun.*, 1999, **163**, 95–102.
10 J. R. DeVore, Refractive Indices of Rutile and Sphalerite, *J. Opt. Soc. Am.*, 1951, **41**, 416–417.
11 C. Chen and Y. Wang, Design and synthesis of an ultraviolet-transparent nonlinear optical crystal $Sr_2Be_2B_2O_7$, *Nature*, 1995, **373**, 322–324.
12 F. Kong, C.-L. Hu, M.-L. Liang and J.-G. Mao, $Pb_4(OH)_4(BrO_3)_3NO_3$: An example of SHG crystal in metal bromates containing π-conjugated planar triangle, *Inorg. Chem.*, 2016, **55**, 948–955.
13 Y. Li, X. Zhang, Y. Zhou, W. Huang, Y. Song, H. Wang, M. Li, M. Hong, J. Luo and S. Zhao, An Optically Anisotropic Crystal with Large Birefringence Arising from Cooperative π Orbitals, *Angew. Chem.*, 2022, **134**, e202208811.

14 D. Lin, M. Luo, C. Lin, F. Xu and N. Ye, KLi($HC_3N_3O_3$)·$2H_2O$: Solvent-drop grinding method toward the hydro-isocyanurate nonlinear optical crystal, *J. Am. Chem. Soc.*, 2019, **141**, 3390–3394.

15 Y. Liu, X. Liu, S. Liu, Q. Ding, Y. Li, L. Li, S. Zhao, Z. Lin, J. Luo and M. Hong, An Unprecedented Antimony(III) Borate with Strong Linear and Nonlinear Optical Responses, *Angew. Chem., Int. Ed.*, 2020, **59**, 7793–7796.

16 V. P. Solntsev, E. G. Tsvetkov, V. A. Gets and V. D. Antsygin, Growth of α-BaB_2O_4 single crystals from melts at various compositions: comparison of optical properties, *J. Cryst. Growth*, 2002, **236**, 290–296.

17 J. Lu, Y.-K. Lian, L. Xiong, Q.-R. Wu, M. Zhao, K.-X. Shi, L. Chen and L.-M. Wu, How to maximize birefringence and nonlinearity of π-conjugated cyanurates, J. Am. Chem. Soc, ., 2019, **141**, 16151–16159.

18 L. Liu, C.-L. Hu, Z. Bai, F. Yuan, Y. Huang, L. Zhang and Z. Lin, $2(C_3H_7N_6)^+ \cdot 2Cl^- \cdot H_2O$: an ultraviolet nonlinear optical crystal with large birefrigence and strong second-harmonic generation, *Chem. Commun.*, 2020, **56**, 14657–14660.

19 Y. Li, J. Luo and S. Zhao, Local Polarity-Induced Assembly of Second-Order Nonlinear Optical Materials, *Acc. Chem. Res.*, 2022, 8560–8563.

20 A. Walsh, D. J. Payne, R. G. Egdell and G. W. Watson, Stereochemistry of post-transition metal oxides: revision of the classical lone pair model, *Chem. Soc. Rev.*, 2011, **40**, 4455–4463.

21 X. Chen, B. Zhang, F. Zhang, Y. Wang, M. Zhang, Z. Yang, K. R. Poeppelmeier and S. Pan, Designing an excellent deep-ultraviolet birefringent material for light polarization, *J. Am. Chem. Soc.*, 2018, **140**, 16311–16319.

22 Q. Jing, Z. Yang, S. Pan and D. Xue, Contribution of lone-pairs to birefringence affected by the Pb(II) coordination environment: a DFT investigation, *Phys. Chem. Chem. Phys.*, 2015, **17**, 21968–21973.

23 Y. Yang, Y. Qiu, P. Gong, L. Kang, G. Song, X. Liu, J. Sun and Z. Lin, Lone–Pair Enhanced Birefringence in an Alkaline–Earth Metal Tin(II) Phosphate $BaSn_2(PO_4)_2$, *Chem. – Eur. J.*, 2019, **25**, 5648–5651.

24 X. Dong, L. Huang, C. Hu, H. Zeng, Z. Lin, X. Wang, K. M. Ok and G. Zou, $CsSbF_2SO_4$: an excellent ultraviolet nonlinear optical sulfate with a $KTiOPO_4$ (KTP)-type structure, *Angew. Chem.*, 2019, **131**, 6598–6604.

25 J. Guo, A. Tudi, S. Han, Z. Yang and S. Pan, Sn2PO4I: An Excellent Birefringent Material with Giant Optical Anisotropy in Non π-Conjugated Phosphate, *Angew. Chem.*, 2021, **133**, 25105–25108.

26 W. Huang, X. Zhang, Y. Li, Y. Zhou, X. Chen, X. Li, F. Wu, M. Hong, J. Luo and S. Zhao, A Hybrid Halide Perovskite Birefringent Crystal, *Angew. Chem., Int. Ed.*, 2022, e202202746.

27 I. H. Park, L. Chu, K. Leng, Y. F. Choy, W. Liu, I. Abdelwahab, Z. Zhu, Z. Ma, W. Chen and Q. H. Xu, Highly Stable Two-Dimensional Tin(II) Iodide Hybrid Organic-Inorganic Perovskite Based on Stilbene Derivative, *Adv. Funct. Mater.*, 2019, **29**, 1904810.

28 A. Bala and V. Kumar, Role of Ligand–Ligand Interactions in the Stabilization of Thin Layers of Tin Bromide Perovskite: An Ab Initio Study of the Atomic and Electronic Structure, and Optical Properties, *J. Phys. Chem. C*, 2019, **123**, 25176–25184.

29 Y. Gao, Z. Wei, P. Yoo, E. Shi, M. Zeller, C. Zhu, P. Liao and L. Dou, Highly stable lead-free perovskite field-effect transistors incorporating linear π-conjugated organic ligands, *J. Am. Chem. Soc.*, 2019, **141**, 15577–15585.

30 F. Wu, Q. Wei, X. Li, Y. Liu, W. Huang, Q. Chen, B. Li, J. Luo and X. Liu, Cooperative Enhancement of Second Harmonic Generation in an Organic–Inorganic Hybrid Antimony Halide, *Cryst. Growth Des.*, 2022, **22**, 3875–3881.

31 T. Tong, M.-H. Lee and J. Zhang, Transformation of optical anisotropy origins in perovskite-related materials: A first-principles study, *J. Phys. Chem. C*, 2019, **123**, 31167–31174.

32 S. Clark, M. Segall, C. Pickard and P. Hasnip, MI ARTICLE Journal Name Probert, K. Refson and MC Payne, *Z. Kristallogr. – Cryst. Mater.*, 2005, **220**, 567–570.

33 W. Kohn, Electronic structure of matter-wave functions and density functionals, *Rev. Mod. Phys.*, 1999, **71**, 1253–1266.

34 L. H. Nicholls, F. J. Rodríguez-Fortuño, M. E. Nasir, R. M. Córdova-Castro, N. Olivier, G. A. Wurtz and A. V. Zayats, Ultrafast synthesis and switching of light polarization in nonlinear anisotropic metamaterials, *Nat. Photonics*, 2017, **11**, 628–633.

35 Y. Li, C. Yin, X. Yang, X. Kuang, J. Chen, L. He, Q. Ding, S. Zhao, M. Hong and J. Luo, A nonlinear optical switchable sulfate of ultrawide bandgap, *CCS Chem.*, 2021, **3**, 2298–2306.

36 L. Wu, S. Patankar, T. Morimoto, N. L. Nair, E. Thewalt, A. Little, J. G. Analytis, J. E. Moore and J. Orenstein, Giant anisotropic nonlinear optical response in transition metal monopnictide Weyl semimetals, *Nat. Phys.*, 2017, **13**, 350–355.

37 C. Jin, F. Lin, Z. Yang, S. Pan and M. Mutailipu, $[C_3N_6H_7]_2[B_3O_3F_4(OH)]$: a new hybrid birefringent crystal with strong optical anisotropy induced by mixed functional units, *J. Mater. Chem. C*, 2022, **10**, 6590–6595.

